

Structures of Cytochrome P450 2B6 Bound to 4-Benzylpyridine and 4-(4-Nitrobenzyl)pyridine: Insight into Inhibitor Binding and Rearrangement of Active Site Side Chains

Manish B. Shah, Jaime Pascual, Qinghai Zhang, C. David Stout, and James R. Halpert

Skaggs School of Pharmacy and Pharmaceutical Sciences (M.B.S., J.P., J.R.H.), University of California, San Diego, La Jolla, California; and Department of Molecular Biology (Q.Z., C.D.S.), the Scripps Research Institute, La Jolla, California

Received June 23, 2011; accepted August 29, 2011

ABSTRACT

The biochemical, biophysical, and structural analysis of the cytochrome P450 2B subfamily of enzymes has provided a wealth of information regarding conformational plasticity and substrate recognition. The recent X-ray crystal structure of the drug-metabolizing P450 2B6 in complex with 4-(4-chlorophenyl)imidazole (4-CPI) yielded the first atomic view of this human enzyme. However, knowledge of the structural basis of P450 2B6 specificity and inhibition has remained limited. In this study, structures of P450 2B6 were determined in complex with the potent inhibitors 4-benzylpyridine (4-BP) and 4-(4-nitrobenzyl)pyridine (4-NBP). Comparison of the present structures with the previous P450 2B6-4-CPI complex showed that reorientation of side chains of the active site residue Phe206 on the F-helix and Phe297 on the I-helix was necessary to accommo-

date the inhibitors. However, P450 2B6 does not require any major side chain rearrangement to bind 4-NBP compared with 4-BP, and the enzyme provides no hydrogen-bonding partners for the polar nitro group of 4-NBP within the hydrophobic active site. In addition, on the basis of these new structures, substitution of residue 172 with histidine as observed in the single nucleotide polymorphism Q172H and in P450 2B4 may contribute to a hydrogen bonding network connecting the E- and I-helices, thereby stabilizing active site residues on the I-helix. These results provide insight into the role of active site side chains upon inhibitor binding and indicate that the recognition of the benzylpyridines in the closed conformation structure of P450 2B6 is based solely on hydrophobicity, size, and shape.

Introduction

Cytochrome P450 (P450)-dependent monooxygenases are a superfamily of heme-containing enzymes that metabolize a wide variety of xenobiotics including many drugs (Johnson and Stout, 2005). The importance of studies of P450 enzymes is bolstered by their critical role in steroid and prostaglandin synthesis in humans. P450 catalysis generally occurs through the insertion of an atom of molecular oxygen into an organic ligand, often in a regio- and stereoselective manner.

This research was supported by National Institutes of Health National Institute of Environmental Health Sciences [Grant ES003619] (to J.R.H.); and National Institutes of Health National Institute of General Medical Sciences [Grant GM073197] (to Q.Z.).

Article, publication date, and citation information can be found at <http://molpharm.aspetjournals.org>.
doi:10.1124/mol.111.074427.

However, these enzymes are also known for the remarkable plasticity that enables them to adapt to and accommodate a broad range of substrates of different size, shape, and stereochemistry (Domanski and Halpert, 2001a; Gay et al., 2010a). As elucidated by crystallographic studies, substrate recognition in P450s is enabled through the repositioning of active site residues and other conformational changes (Williams et al., 2000). The structural analysis of rabbit P450 2B4 in complex with the drugs ticlopidine and clopidogrel is a recent illustration of such side chain rearrangement to accommodate the respective ligands within the active site (Gay et al., 2010b).

Human P450 2B6 metabolizes a large pool of clinically important drugs including bupropion, efavirenz, cyclophosphamide, selegiline, propofol, and artemisinin (Zanger et al., 2007). Despite major advances in crystallization and struc-

ABBREVIATIONS: P450, cytochrome P450; P450 2B6, an N-terminally truncated and modified and C-terminally His-tagged form of the cytochrome P450 2B6 genetic variant K262R with an internal mutation at position 226; SNP, single nucleotide polymorphism; 4-CPI, 4-(4-chlorophenyl)imidazole; 4-BP, 4-benzylpyridine; 4-NBP, 4-(4-nitrobenzyl) pyridine; 7-EFC, 7-ethoxy-(4-trifluoromethyl)coumarin; CHAPS, 3-[(3-cholamidopropyl)dimethylammonio]-1-propanesulfonic acid; 234-chol, 3R-hydroxy-7R,12R-bis(2-(tri-methylamino)ethyl)phosphoryl)ethoxy)cholane; BME, 2-mercaptoethanol; PMSF, phenylmethylsulfonyl fluoride; DTT, dithiothreitol; PDB, Protein Data Bank; RMSD, root mean square deviation; tBPA, *tert*-butylphenylacetylene.

tural biology of human P450 enzymes, direct structural information on P450 2B6 has remained scant. Moreover, the polymorphic nature of P450 2B6 results in several variants, including the most common single nucleotide polymorphisms (SNPs) Q172H and K262R (Zanger et al., 2007), which lead to differences in protein levels and/or activity among individual organisms. Detailed information on P450 2B6 structure-activity relationships will be required to understand the mechanisms of altered protein function.

Over the past decade, more than 10 structures of P450 2B4, which shares 78% amino acid sequence identity with P450 2B6, were solved, revealing four different conformations. These include two distinct ligand-free states of protein, open and closed, as well as other conformations observed in complex with various inhibitors and drugs (Gay et al., 2010a). The crystal structures of the open ligand free form and two inhibitor-bound complexes were in agreement with the conformational changes observed in solution in recent hydrogen-deuterium exchange mass spectrometry experiments (Wilderman et al., 2010). Furthermore, the flexible regions of 2B4 affected by ligand binding were consistent between the solution studies and X-ray crystal structures. Until recently, the structures of rabbit P450 2B4 served as a template for making homology models and for identifying key residues in human P450 2B6 (Domanski and Halpert, 2001a; Kumar et al., 2007). The recently determined crystal structure of a P450 2B6 genetic variant in complex with 4-(4-chlorophenyl)imidazole (4-CPI) provided a detailed look at this human enzyme (Gay et al., 2010c), which allowed for the comparison of two P450 2B structures from different species. Here, Y226H and K262R mutations were introduced into the wild-type P450 2B6 construct with an N-terminal truncation and modifications. These internal mutations were made on the basis of years of research efforts to improve the stability, solubility, and yield of this enzyme, making it amenable for the high expression levels and purity required for crystallization (Hanna et al., 2000; Scott et al., 2001; Mitsuda and Iwasaki, 2006; Kumar et al., 2007).

To further our understanding of structure-function relationships in P450 2B6 and its role in drug metabolism and interactions, we solved the crystal structures of P450 2B6 in complex with the inhibitors 4-benzylpyridine (4-BP) and 4-(4-nitrobenzyl) pyridine (4-NBP). The in vitro inhibition potency of various pyridine inhibitors and other structurally unrelated compounds has been determined previously using 7-ethoxy-4-trifluoromethylcoumarin (7-EFC) as the substrate with recombinant wild-type 2B6 and also with human liver microsomes (Korhonen et al., 2007). From these studies, 4-BP and 4-NBP were proposed as potent and selective P450 2B6 inhibitors of potential use in drug design and development (Korhonen et al., 2007). Our study compares the structures of P450 2B6 complexes with 4-BP, 4-NBP, and 4-CPI structure, enabling us to analyze specific reorientations of amino acid side chains to facilitate ligand binding within the mostly hydrophobic active site.

Materials and Methods

Materials. 4-BP and 4-NBP were from Sigma-Aldrich (St. Louis, MO). CHAPS was from Calbiochem (San Diego, CA). Cymal-5 (5-cyclohexyl-1-pentyl- β -D-maltoside) was from Anatrace (Maumee, OH). Amicon ultrafiltration devices were from Millipore Corporation (Bil-

lerica, MA). The Index HT crystal screen was obtained from Hampton Research (Aliso Viejo, CA). Nickel-nitrilotriacetic acid affinity resin was from QIAGEN (Valencia, CA). Macro-Prep CM cation exchange resin was from Bio-Rad Laboratories (Hercules, CA). The pGro7 plasmid was acquired from Takara Bio (Shiba, Japan). *Escherichia coli* JM109 cells were from Stratagene (La Jolla, CA). 3*R*-Hydroxy-7*R*,12*R*-bis((2-(trimethylamino)ethyl)phosphoryl)ethoxy)cholane (234-chol) is a custom-made new facial amphiphile (Zhang et al., 2007). All figures were created using PyMOL (DeLano, 2002). BKchem version 0.13.0 (2009; <http://bkchem.zirael.org/index.html>) was used for drawing the chemical structures of 4-BP and 4-NBP.

Protein Expression and Purification. Heterologous expression of P450 2B6 was done similarly to a protocol described previously (Scott et al., 2001). In brief, an overnight Luria-Bertani broth culture of *E. coli* JM109 cells containing the pKK2B6 plasmid was used to inoculate Terrific broth. GroEL/ES chaperones (pGro7 plasmid) were coexpressed with the pKK2B6 plasmid containing the cDNA for 2B6 (Y226H/K262R) in the presence of chloramphenicol and ampicillin. Terrific broth cultures were grown until A_{600} reached approximately 0.7 at 37°C. Protein expression was induced for 72 h at 30°C by addition of isopropyl β -D-1-thiogalactopyranoside and δ -aminolevulinic acid to final concentrations of 0.5 and 1 mM, respectively. Cells were harvested by centrifugation and resuspended in 10% of the original culture volume in buffer containing 20 mM potassium phosphate (pH 7.4 at 4°C), 20% (v/v) glycerol, 10 mM BME, and 0.5 mM PMSF. After treatment with lysozyme (0.2 mg/ml), the suspension was again collected by centrifugation. The resulting spheroplasts were then resuspended in the buffer containing 500 mM potassium phosphate (pH 7.4 at 4°C), 20% (v/v) glycerol, 10 mM BME, and 0.5 mM PMSF and were sonicated three times for 45 s on ice. The detergent CHAPS was then added at a final concentration of 0.8% (w/v), and the solution was allowed to stir for 90 min at 4°C before it was subjected to ultracentrifugation for 45 min at 245,000g in an Optima L-80 XP ultracentrifuge using a Ti 50.2 rotor (Beckman Coulter, Fullerton, CA). The concentration of P450 in the supernatant was measured using the reduced CO difference spectra (Omura and Sato, 1964).

Nickel affinity chromatography was used for the purification of histidine-tagged 2B6 performed in the presence of CHAPS. Protein bound to the nickel-nitrilotriacetic acid column was washed using buffer containing 100 mM potassium phosphate (pH 7.4 at 4°C), 100 mM NaCl, 20% (v/v) glycerol, 10 mM BME, 0.5 mM PMSF, 0.5% CHAPS, and 5 mM histidine. The protein was eluted using buffer containing 10 mM potassium phosphate (pH 7.4 at 4°C), 100 mM NaCl, 20% (v/v) glycerol, 10 mM BME, 0.5 mM PMSF, 0.5% CHAPS, and 50 mM histidine. The pooled P450-containing fractions were collected and then loaded onto a Macro-Prep CM column. The column was washed using the buffer containing 20 mM NaCl, and the protein was eluted with high-salt buffer containing 50 mM potassium phosphate (pH 7.4 at 4°C), 500 mM NaCl, 20% (v/v) glycerol, 1 mM EDTA, and 0.2 mM DTT. Protein fractions containing the highest A_{417}/A_{280} ratios were pooled, and the P450 concentration was measured using the reduced CO difference spectra (Omura and Sato, 1964).

Crystallization and Data Collection. Two milliliters of the pooled purified protein (150 μ M) was diluted to 18 μ M in 50 mM potassium phosphate, pH 7.4, 500 mM sucrose, 500 mM NaCl, 1 mM EDTA, and 0.2 mM DTT. This solution was divided into two equal aliquots, and either 4-BP or 4-NBP was added to a final concentration of 180 μ M. To exchange the glycerol with sucrose, the protein was concentrated to 275 μ M by centrifugation using 50-kDa molecular mass cutoff Amicon ultrafiltration devices. The protein was again diluted to 18 μ M with the above buffer containing the respective ligand at a concentration of 180 μ M. This process was repeated twice before the individual aliquots of the 2B6-4-BP and 2B6-4-NBP complexes were concentrated to a final concentration of 275 μ M. The concentrated protein was supplemented with 4.8 mM Cymal-5, 0.028% (w/v) 234-chol, and either 1 mM 4-BP or 1 mM 4-NBP.

Sitting drop vapor diffusion was used to screen crystal conditions using the Hampton Research Index HT crystallization screen. Crystals of 2B6-4-BP were obtained at 18°C after 5 days of incubating the protein in a 1:1 ratio with a solution containing 0.2 M ammonium acetate, 0.1 M HEPES, pH 7.5, and 20% (w/v) PEG 3350. Crystals of 2B6-4-NBP grew over a period of 7 days in a fashion similar to that described above using a solution containing 0.15 M DL-malic acid, pH 7.0, and 20% (w/v) PEG 3350. The inclusion of the novel facial amphiphile 234-chol during crystallization trials helped to achieve high-quality, well diffracting crystals. Tests of another facial amphiphile, 232-chol (Zhang et al., 2007), with the same screen gave crystals, but they diffracted to poor resolution (>6 Å). It is noteworthy that our attempts to grow crystals in the absence of facial amphiphiles yielded either no crystals or crystals that are too small to diffract, similar to our previous observations in the crystallization of 2B6-4-CPI (Gay et al., 2010c).

Crystals of 2B6-4-BP were transferred to a solution containing 25 mM potassium phosphate, pH 7.4, 250 mM NaCl, 0.5 mM EDTA, 0.1 mM DTT, 0.1 M ammonium acetate, 50 mM HEPES, 10% (w/v) PEG 3350, 2.4 mM Cymal-5, and 500 mM sucrose for cryoprotection. The crystals of 2B6-4-NBP were transferred to a cryoprotection solution similar to that described above, which contained 75 mM DL-malic acid in place of 0.1 M ammonium acetate and 50 mM HEPES. Crystals were flash-frozen in liquid nitrogen, and the crystallographic data were collected remotely at Stanford Synchrotron Radiation Laboratory beamline 11-1 (Soltis et al., 2008) using 0.5° oscillations over 180 frames and 10-s exposures. Crystals of 2B6 in complex with 4-BP and 4-NBP diffracted to 2.1 and 2.8 Å, respectively, and the data were integrated using iMOSFLM (Leslie, 1999) and scaled via SCALA in CCP4 (Collaborative Computational Project and Number 4, 1994) (Table 1).

Structure Determination and Refinement. Structure solutions were suggested using the automated molecular-replacement

TABLE 1

Data collection and refinement statistics

Values for the highest resolution shell are shown in parentheses.

Construct	2B6 (Y226H/K262R)	
Ligands	4-BP	4-NBP
Crystal space group	P3 ₂ 21	P3 ₂
Crystal unit cell parameters		
a = b, Å	76.8	101.9
c, Å	201.3	299.5
α = β, °	90	90
γ, °	120	120
Molecules per asymmetric unit	1	6
Data collection statistics		
Beamline	SSRL 11-1	SSRL 11-1
Wavelength, Å	0.98	0.98
Resolution range, Å	50.3–2.1	84.6–2.8
Completeness, %	91.7 (92.4)	88.9 (78.6)
Redundancy	4.0 (3.8)	2.6 (2.4)
R _{merge} , %	12.4 (43)	6.3 (36)
I/σ	4.3 (1.7)	9.6 (2.1)
No. of unique reflections	37,630	76,085
Refinement statistics		
R factor, %	19.7	21.8
R _{free} , %	25.0	25.9
RMSDs		
Bond lengths, Å	0.022	0.018
Bond angles, °	1.87	1.719
No. of atoms		
Protein	3711	22,228
Heme	43	258
Ligand	13	56
Waters	250	150
Detergent	18	272
Average B factor, Å ²	23.4	52.7
Ramachandran plot		
Preferred, %	98	95.3
Allowed, %	100	99.8

SSRL, Stanford Synchrotron Radiation Laboratory.

pipeline BALBES (Long et al., 2008). Clearly defined unbiased electron density for each of the respective ligands was observed in maps based on the individual output models from BALBES. Library descriptions for the ligands were created using the PRODRG server (van Aalten et al., 1996). The Matthews' coefficient suggested the presence of one molecule in the asymmetric unit for the 2B6-4-BP structure and six molecules in the asymmetric unit for the 2B6-4-NBP structure. The output models from BALBES were further subjected to iterative model building with COOT (Emsley and Cowtan, 2004) using F_o – F_c and 2F_o – F_c electron density maps contoured at 3σ and 1σ, respectively. Water and Cymal-5 molecules were located and added manually, and REFMAC5 (Murshudov et al., 1997) was used for a rigid body and a restrained refinement until the completion of the model (Table 1). The final models were validated using the program MOLPROBITY (Davis et al., 2004), and the overall geometry ranked in the 94th percentile for the 4-BP complex and 98th percentile for the 4-NBP complex among structures of comparable resolution. Atomic coordinates and structure factors for the individual structures were deposited in the Protein Data Bank (PDB entries 3QOA and 3QU8 for the 4-BP and 4-NBP complexes, respectively).

Spectral Studies of 4-BP and 4-NBP Binding to 2B6. Titrations were performed in buffer containing 50 mM potassium phosphate, pH 7.4, 500 mM NaCl, 1 mM EDTA, 0.2 mM DTT, and 500 mM sucrose. Inhibitors (4-BP or 4-NBP) were dissolved in acetone, and the total solvent concentration maintained in the titration experiments was less than 1%. Difference spectra were recorded at room temperature after the addition of the inhibitor (100 μM stock concentration) to buffer containing 1 μM P450 in a 1-ml reaction volume on an S2000 single-channel charge-coupled device rapid scanning spectrophotometer (Ocean Optics, Inc., Dunedin, FL) using a 1-cm glass cuvette with a magnetic stirring compartment (Hellma USA, Plainview, NY) as described previously (Gay et al., 2010b). To determine the spectral binding constants (K_D) of these high-affinity inhibitors, the data were fit to the "tight binding" equation: $2\Delta A = (\Delta A_{\max}/[E_0]) - [K_D + [I_0] + [E_0] + (K_D + [I_0] + [E_0])^2 - (4[I_0][E_0])^{1/2}]$, where ΔA was the difference in absorbance between the maxima and minima, and [E₀] and [I₀] are total enzyme and total inhibitor concentrations, respectively (Segel, 1975).

IC₅₀ Determinations. 7-EFC O-deethylation to the metabolite 7-hydroxy-4-trifluoromethylcoumarin was measured using a fluorometric assay. The reconstituted system contained the following recombinant proteins at a molar ratio of 1:4:2: 2B6, rat cytochrome P450 reductase (Harlow and Halpert, 1997), and rat cytochrome b₅ (Holmans et al., 1994). The respective inhibitors were dissolved in acetone, and the total solvent content was maintained below 1% in the reaction mixture. Each 100-μl reaction mixture contained 50 mM HEPES, pH 7.4, 15 mM MgCl₂, 10 pmol of P450, 40 pmol of cytochrome P450 reductase, 20 pmol of cytochrome b₅, 50 μM 7-EFC, and 0 to 100 μM either 4-BP or 4-NBP. NADPH was added to initiate the reaction after 5 min of preincubation at 37°C. The reactions were terminated by adding 20% trichloroacetic acid after 5 min of incubation. A control experiment was performed by quenching the reaction in the absence of substrate. Fluorescence was measured using an F-2000 fluorescence spectrophotometer (Hitachi, Tokyo, Japan) with excitation at 410 nm and emission at 500 nm. The IC₅₀ values were determined using the tight binding equation with the scientific analysis package Igor Pro 6.1 (Wavemetrics, Inc., Lake Oswego, OR).

Results

Structure of 2B6 (Y226H/K262R) in Complex with 4-BP. The 2B6-4-BP complex crystallized in the P3₂21 space group with one molecule in the asymmetric unit. The structure of 2B6-4-BP was determined using BALBES, which used the structure of the 2B4-clopidogrel complex (Gay et al., 2010b) as the search model from the PDB database (PDB code 3ME6). The 2B6-4-BP output model was modified to

reflect the amino acid differences between the 2B4 and 2B6 sequences. The inhibitor 4-BP with the pyridine nitrogen bound to the heme iron was clearly defined in an unbiased electron density map, and the inhibitor was modeled just before the final rounds of refinement (Fig. 1A). The iterative process of model building and refinement using COOT and REFMAC5 resulted in a final R factor and R_{free} of 19.7 and 25.0%, respectively (Table 1). The crystal structure of P450 2B6 bound to 4-BP is shown in Fig. 1B. The protein residues from Gly28 through the first residue of the C terminus, engineered 4X His tag (His492) were ordered except for the stretch from Phe136 to Arg140. Moreover, the mutations Y226H and K262R, which were introduced for enhanced solubility and stability, as described previously (Gay et al., 2010c), were also clearly defined in the electron density. As observed in the 2B6-4-CPI complex, the polymorphic mutation K262R forms hydrogen bonds with residues Thr255 and Asp266 to possibly help stabilize the G/H loop. The model also contains 249 water molecules and two partially occupied molecules of Cymal-5. The density for the maltose group was not observed for one Cymal-5 molecule located near Phe220 and Phe223, and the density for only the cyclohexane ring was observed for the other molecule of Cymal-5 in the hydrophobic pocket near residues Leu43, Val212, and Leu216.

Structure of P450 2B6 (Y226H/K262R) in Complex with 4-NBP. Six molecules in the asymmetric unit were present in the 2B6-4-NBP structure, which crystallized in the $P3_2$ space group. BALBES selected the 2B6-4-CPI complex (Gay et al., 2010c) as the most closely related structure from the PDB database (PDB code 3IBD). Unbiased electron density from REFMAC5 clearly showed that 4-NBP bound to the heme iron in chain B (Fig. 1C). However, in the other five copies, 4-NBP displayed varying degrees of disorder with partial density for the inhibitor. Density for the anionic nitro group of 4-NBP was not present in chains D and E, and the density for the nitrobenzyl moiety was missing in chains A and C. The density for 4-NBP was the poorest in chain F, and the ligand was not modeled in the active site. Despite these differences in the degree of order of 4-NBP, the six copies of the protein were very similar (RMSD of 0.144 Å in a $C\alpha$ overlay). The crystal structure of 2B6-4-NBP is shown in Fig. 1D.

Overall, residues from Gly28 to His492 were observed in the final model in chains A, B, C, D, and E, whereas chain F consisted of residues Gly28 to Ile486. As in the 4-BP structure, residues from Phe136 to Arg140 were disordered in each chain of this structure. Of interest, these residues lie within the C–D loop region of 2B6, which was previously reported to interact with cytochrome P450 reductase (Bum-

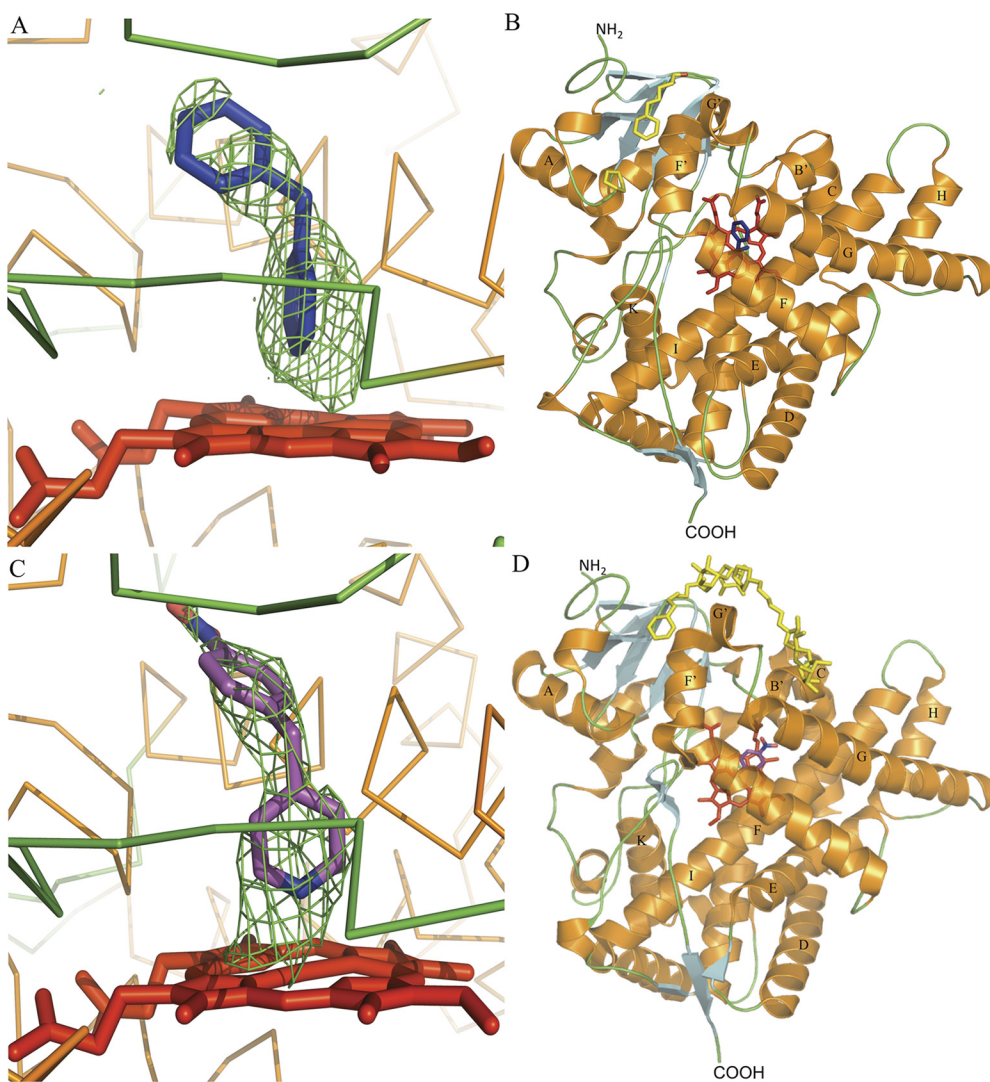


Fig. 1. Electron density maps and structures of 4-BP and 4-NBP bound to 2B6. Heme is shown in red, and the inhibitors 4-BP and 4-NBP are shown in blue and magenta sticks, respectively. A, an unbiased F_o-F_c omit map calculated before inclusion of the inhibitor in the 2B6-4-BP structure contoured at 3σ shows electron density corresponding to 4-BP above the heme. B, ribbon diagram of 2B6-4-BP complex structure. Labeled α -helices are shown in orange and β -sheets are shown in cyan. Two partial Cymal-5 detergent molecules are shown in yellow sticks. C, a similar F_o-F_c omit map for the 2B6-4-NBP structure (chain B) contoured at 3σ shows electron density corresponding to 4-NBP above the heme. D, ribbon diagram of the 2B6-4-NBP complex (chain B). Labeled α -helices are shown in orange and β -sheets are shown in cyan. Two Cymal-5 detergent molecules are shown in yellow sticks.

pus and Hollenberg, 2010). Arg262 was observed interacting with the same residues as in the 2B6-4-BP and 2B6-4-CPI structures.

Comparison of the 2B6-4-BP and 2B6-4-NBP Structures. With their predominant α -helical domains aligning very closely, the closed conformation structures of 2B6 in complex with 4-BP and with 4-NBP are nearly identical, with an RMSD of 0.302 Å in a C α overlay. A total of 14 residues, located mainly on the B/C loop and helices F and I, found within a 5 Å radius of either 4-BP or 4-NBP make up the active site of the enzyme (Fig. 2A). These include all the residues previously shown to interact with the ligand in the 2B6 and 2B4 complexes with 4-CPI (Scott et al., 2004; Gay et al., 2010c) and additional residues Leu362 in the 2B6-4-BP and Phe108 in the 2B6-4-NBP structures, respectively. The heterocyclic nitrogen of the pyridine ring bound to heme in the 2B6-4-BP structure rotates by approximately 90° in the 2B6-4-NBP structure. Moreover, the benzyl group of 4-NBP shifts by approximately 40° to accommodate the additional polar nitro group, and this displaces residue Phe108 away from its observed location in the 2B6-4-BP structure (Fig. 2A). Such positioning of the nitrobenzyl group of 4-NBP allows for inclusion of an additional active site residue, Phe108, located within the 5 Å radius from the ligand. The lack of any hydrogen bonding partners to interact with the nitro group could help explain the poor electron density observed for the nitro and nitrobenzyl groups in chains A, C, D, E, and F in the 2B6-4-NBP structure. Furthermore, small movements of residues Phe108, Phe115, Phe206, Phe292, and Phe297 compared with the 2B6-4-BP structure result in

an increase of active site cavity volume from 279 Å³ in 2B6-4-BP to 344 Å³ for 2B6-4-NBP, as calculated by VOIDOO (Kleywegt and Jones, 1994). The change in cavity volumes resulted mainly from the movement of the above residues to accommodate the bulkier 4-NBP ligand in the active site. However, the side chain of Leu362 in the 2B6-4-BP structure also protrudes by approximately 90° toward the active site and pushes Thr302 in close proximity to the pyridine ring of 4-BP (Fig. 2A), which further reduces the active site cavity volume in the 2B6-4-BP structure.

Comparison with the 2B6-4-CPI Structure. An overlay of 2B6-pyridine and 2B6-4-CPI structures results in RMSDs of 0.66 and 0.54 Å for the 2B6-4-BP and 2B6-4-NBP structures, respectively. The differences between the structures of the 2B6-4-CPI complex and the 2B6-4-BP and 4-NBP complexes result mainly from movement of residues within the active site to accommodate the different ligands. Phe297 on the I-helix, which protrudes into the active site in the 2B6-4-CPI structure, moves away to make space for the kinked structures of 4-NBP and 4-BP. This forces Phe206 on the F-helix to move by approximately 90° toward Val477 (Fig. 2B). In the 2B6-pyridine inhibitor complexes, Val104, Phe115, and Glu301 are located within a 5 Å radius of the ligand but were found slightly outside of this radius in the 2B6-4-CPI structure. In addition, the side chain of Glu301 in the 2B6-4-BP and 4-NBP structures flips out of the active site and contacts a water molecule as seen in the 2B6-4-CPI structure.

Spectral Binding and Enzyme Inhibition Studies. Addition of 4-BP and 4-NBP yielded type II difference spectra

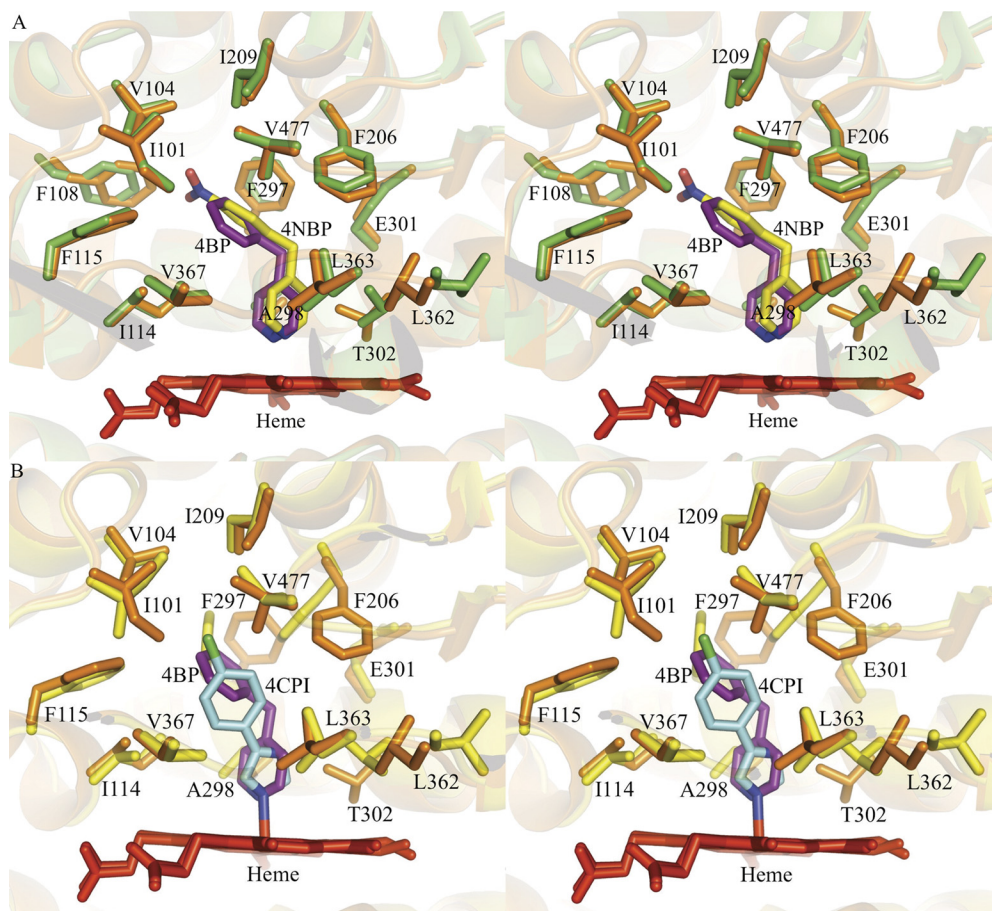


Fig. 2. Superimposed structures of 2B6 complexes in stereo view showing active site residues in sticks found within a 5-Å radius of the ligand. Heme is shown in red, and 4-BP, 4-NBP, and 4-CPI ligands are shown in purple, yellow, and cyan, respectively. A, an overlay of the 2B6-4-BP (orange) and 2B6-4-NBP (green) structures showing the binding of 4-BP and the accommodations near Phe108 required for binding of the more polar 4-NBP. The residues that comprise the binding site in both complexes are Ile101, Val104, Ile114, Phe115, Phe206, Ile209, Phe297, Ala298, Glu301, Thr302, Leu363, Val367, and Val477. New active site residues were identified in each structure: Leu362 for the 2B6-4-BP complex and Phe108 for the P450 2B6-4-NBP complex. B, superposition of the 2B6-4-BP (orange) and 2B6-4-CPI (yellow) structures highlighting the differences in the orientation of active site residues, particularly the side chains of Ile101, Phe115, Phe206, and Phe297.

with a peak at 423 nm and trough at 411 nm. The tight binding equation was used to determine the spectral binding constants for 4-NBP and 4-BP. 2B6 binds both ligands with comparable K_D values of 0.21 and 0.16 μM for 4-BP and 4-NBP, respectively (Table 2). Moreover, the K_D values obtained with this 2B6 (Y226H/K262R) mutant used for crystallization were similar to those determined previously in wild-type 2B6 (Kumar et al., 2007). The IC_{50} values for inhibition of 2B6-catalyzed 7-EFC O-deethylation were 0.18 μM for BP and 0.09 μM for NBP (Table 2), which correspond well with the previously observed values using wild-type cDNA-expressed 2B6 (Korhonen et al., 2007).

Discussion

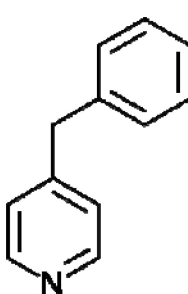
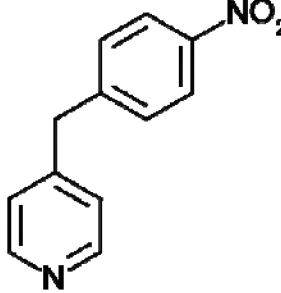
Until recently, crystallographic studies of P450 2B enzymes were mainly focused on rabbit 2B4 because of its optimal solubility and stability during purification and crystallization. A series of crystal structures of 2B4 identified the active site residues that are involved in substrate recognition and ligand binding. In the closed structures of 2B4 in complex with 4-CPI and 1-CPI, residues contacting the ligand include Ile101, Val104, Ile114, Phe115, Phe206, Ile209, Phe297, Ala298, Glu301, Thr302, Ile362, Val367, and Val477, which are mainly hydrophobic except for Glu301 and Thr302 (Scott et al., 2004; Zhao et al., 2007). The corresponding residues in the active site of 2B6 deduced from the 4-CPI complex were essentially the same, with the only substitution occurring at residue 363, which is Ile in 2B4 and Leu in 2B6. In addition, the structure of 2B6 in complex with 4-CPI revealed similarities in the orientations of side chains involved in binding the inhibitor compared with the 2B4–4-CPI complex. The structures of 2B6 in complex with the potent and selective inhibitors 4-BP and 4-NBP show rearrangement of amino acid side chains, particularly those of

phenylalanine residues within the hydrophobic cavity, without affecting the overall conformation of the protein.

The reorientation of Phe206 and Phe297 side chains, along with the movement of Phe108, was found to be crucial to accommodate 4-BP and the bulkier 4-NBP ligand. In the 2B6–4-NBP structure, Phe108 is located within a 5-Å radius of 4-NBP. This residue does not contact ligands in most 2B crystal structures. However, interactions between Phe108 and covalently bound *tert*-butylphenylacetylene (tBPA) in 2B4 were observed recently (Gay et al., 2011). Structural alignment of the active site residues of 2B6–4-NBP with those in 2B6–4-BP revealed that the side chain of Phe108 in the B/C loop region sways away from the active site in the 4-NBP complex to accommodate the nitro moiety of 4-NBP (Fig. 2A). In the 2B6–4-CPI structure, Phe108 shifts toward the G-helix to accommodate the movement of Phe115. The benzyl group of 4-BP points toward residue Phe115 in the active site, whereas the addition of the nitro group in 4-NBP repositions this ligand, which points toward Phe108 on the B'-helix. It is noteworthy that the polarity of the nitro group in 4-NBP did not result in any major rearrangement of residues, but only side chain adjustments in the structure including that of Phe108 located opposite to the I-helix, suggesting that ligand binding is based solely on hydrophobicity, size, and shape.

Among the other phenylalanine residues in the active site, Phe206 and Phe297, which were previously shown to be involved in substrate recognition, adopt conformations similar to those observed in the 2B4–1-CPI, 2B4–clopidogrel, and 2B4–tBPA structures, in which Phe206 moves into the active site and Phe297 moves out. In the 4-BP and 4-NBP structures, this prevents the large aromatic side chains from clashing with the pyridine inhibitors (Fig. 3). In contrast, in the 2B6–4-CPI structure and also 2B4–4CPI, 2B4–ticlopidine, and the closed ligand-free 2B4 structures, these two Phe residues orient themselves in the opposite fashion (Gay

TABLE 2
Determination of K_D and IC_{50} values for 2B6 (Y226H/K262R) with 4-BP and 4-NBP

Ligand	K_D	IC_{50}
	μM	
 4-BP	0.21 ± 0.09	0.18 ± 0.06
 4-NBP	0.16 ± 0.07	0.09 ± 0.03

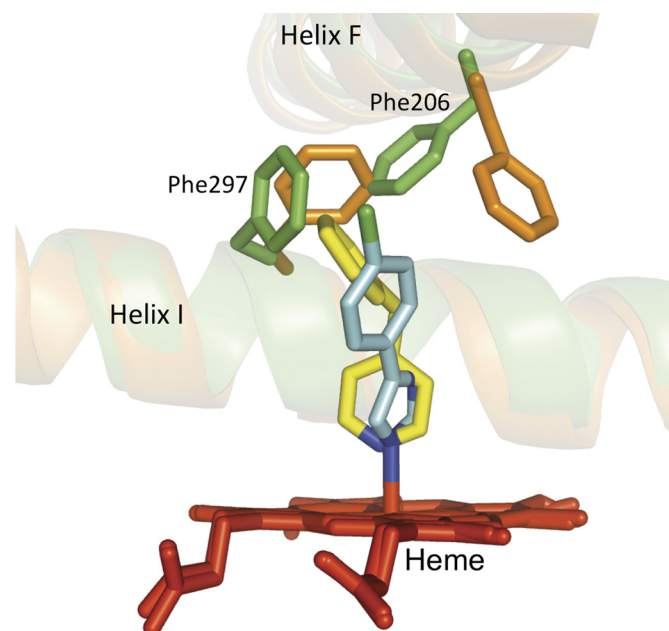


Fig. 3. Ribbon-and-stick diagram showing the orientation of Phe206 and Phe297 on the F- and I-helices, respectively, in the P450 2B6 4-CPI and 4-BP structures. The 2B6–4-BP complex is shown in orange with 4-BP in yellow, and the 2B6–4-CPI structure is shown in green with 4-CPI in cyan.

et al., 2010a). Of interest, substitution of Phe304 in P450 3A4, which is equivalent to Phe297 in P450s 2B, with either alanine or tryptophan has been shown to increase progesterone hydroxylation (Domanski et al., 1998, 2000). In P450 2B1, which shares 78% sequence identity with 2B6, only tryptophan substitution yielded a metabolite profile similar to that of wild-type 2B1, suggesting that an aromatic ring is required at this location for normal substrate binding (Domanski and Halpert, 2001a). The substitution of alanine for Phe297 in 2B1 also decreased the production of the predominant 7-hydroxycoumarin metabolite [7-(5-hydroxyhexoxy) coumarin] to half of that seen in the wild type (Domanski and Halpert, 2001a). Furthermore, a similar study investigated the role of Phe206 in the 2B1 active site by substituting the smaller and more flexible leucine residue. This study reported decreased steroid hydroxylation and altered androstenedione and testosterone profiles, with increased progesterone oxidation (He et al., 1994). This F206L mutation was also shown to reduce the rates of alkoxy coumarin O-dealkylation compared with that of wild-type 2B1 (Kobayashi et al., 1998), whereas F206A in 2B4 showed significantly lower activity toward 7-EFC and thermodynamically unfavorable ligand binding to 1-CPI than the 2B4 wild-type enzyme (Zhao et al., 2007).

From the structural alignment of active site residues in Fig. 2, A and B, it was somewhat surprising to see Leu362 within 5 Å of the inhibitor in the active site of the 2B6-4-BP complex. The side chain of Leu362 flips inward in the active site and toward the pyridine ring of 4-BP, which now rotates 90° compared with the pyridine of 4-NBP and imidazole ring of 4-CPI (Fig. 2, A and B). However, this is seen only in the 2B6-4-BP complex, and such movement also pushes residue Thr302 closer to the ligand than in the other two structures. In addition, structural alignment of all three 2B6 complexes revealed that two water molecules now fill the space in the BP complex otherwise occupied by Leu362 in 2B6-4-CPI and 4-NBP structures. Leu362 has not been observed to interact with ligands in any of the previously solved 2B4 or 2B6 structures. However, Leu362 was analyzed earlier in 2B1, and the substitution with either alanine or phenylalanine caused a dramatic loss in overall activities including steroid

and 7-alkoxycoumarin oxidation (Domanski et al., 2001b). Moreover, the corresponding aligned amino acid residue 365 in the closely related P450 2A4 and 2A5 enzymes is important for the ability to hydroxylate coumarin, and any mutant at this position has exhibited altered substrate specificity (Lindberg and Negishi, 1991).

The active site residue Glu301, with its polar side chain, contributes to ligand binding in the 2B subfamily as evidenced by structural studies. Glu301 in the 2B4-4-CPI structure protrudes from the I-helix toward 4-CPI, where it interacts with the free azole nitrogen of the inhibitor (Scott et al., 2004). In contrast, in the 2B4-1-CPI, 2B4-tBPA (closed), and 2B4-ticlopidine complexes, the same residue moves out of the active site and interacts with His172 (Fig. 4A) (Gay et al., 2010c). In all three 2B6 complexes, Glu301 also flips out of the active site and interacts with Gln172 (Fig. 4B). In the 2B6-4-BP and 2B6-4-CPI structures, Glu301 also interacts with trapped water molecules (waters are not resolved in the 2B6-4-NBP structure) (Fig. 4B). It is noteworthy that the water molecule interacting with Glu301 also contacts the nearby Ser304. Of interest, Ser304 is highly conserved among the 2B subfamily of enzymes (Fig. 5), as well as in other human P450s including 3A4. Therefore, a hydrogen bonding network is conserved for the flipped out conformation of Glu301 that involves direct interaction of Ser304 with His172 in 2B4 and water-mediated interaction when Gln172 is present in 2B6 (Fig. 4, A and B). The lack of direct hydrogen bonding involving Ser304 in 2B6 may weaken the interaction of the E- and I-helices and influence the orientation of active site residues on the I-helix. Moreover, residue 172, which is in close proximity to the active site, is the location of a known 2B6 SNP, resulting in a Q172H substitution (Zanger et al., 2007). Previous studies involving 2B6 Q172H have shown decreased catalytic activity for bupropion hydroxylation and efavirenz metabolism compared with that of the wild type (Zhang et al., 2011). In addition, in most carriers, Q172H is associated with another major SNP, K262R, and the Q172H/K262R variant has shown decreased 2B6 activity and increased plasma concentration of the drug (Desta et al., 2007).

To conclude, the crystal structures of 2B6 in complex with the potent and selective inhibitors 4-BP and 4-NBP revealed

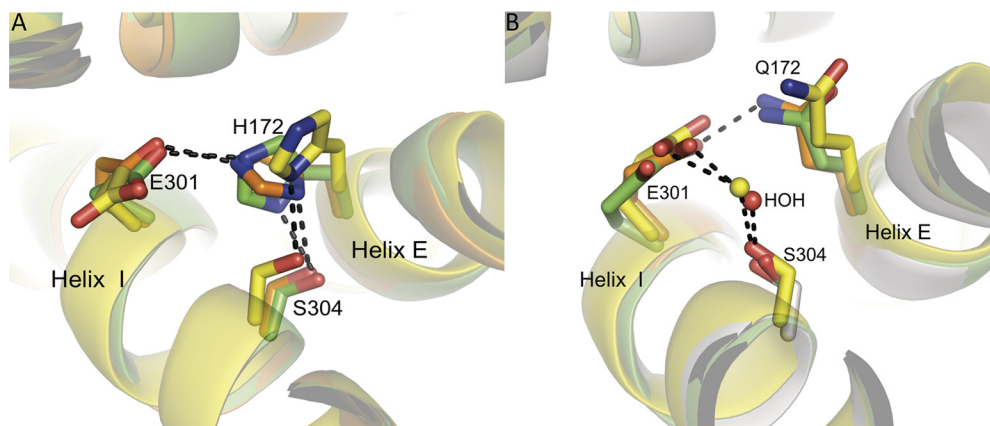


Fig. 4. Ribbon-and-stick representation of structural alignment showing residues 172, 301, and 304 located on helices E and I in 2B4 and 2B6, respectively. Waters are shown as spheres, and dashed lines indicate hydrogen bonds. A, aligned 2B4 structures in complex with 1-CPI (orange), tBPA (closed conformation) (green), and ticlopidine (yellow). The hydrogen-bonding network among His172, Glu301, and Ser304 connects helices E and I and may influence residues in the active site. B, aligned 2B6 structure in complex with 4-CPI (yellow), 4-BP (orange), and 4-NBP (green). A similar interaction of Ser304 with His172 is not seen because of the substitution of His172 with Gln in 2B6, which may affect the hydrogen-bonding network connecting the E and I helices that also include residues within the active site.

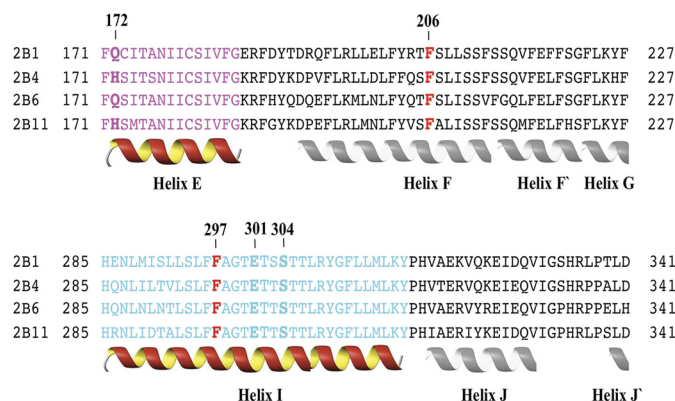


Fig. 5. Multiple sequence alignment of the region in P450 2B1, 2B4, 2B6, and 2B11 showing the location of the SNP at residue 172 on helix E (magenta) and residues Glu301 and Ser304 on helix I (cyan). The highly conserved residues Phe206 and Phe297 are shown in red. Secondary structures, mainly E and I α -helices, as observed from the 2B6 and 2B4 complexes are indicated.

a closed active site comprising amino acid residues that can vary the conformation of their side chains to allow binding of diverse ligands. Such structural rearrangement is observed particularly with the side chains of residues Phe206 and Phe297 (Fig. 3), which were previously implicated in substrate recognition among other P450s including the 2B subfamily of enzymes. Moreover, the highly conserved Ser304 may play an important role in substrate binding by forming a hydrogen-bonding network near the active site. Site-directed mutagenesis with alanine, a non-hydrogen-bonding residue, may help elucidate the role of Ser304 in substrate recognition and activity, both in the 2B6 wild type and in the Q172H variant. Additional crystal structures of 2B6 with larger ligands will be needed to determine the function of other residues, including Leu362, not previously observed within the active site that may contribute to ligand binding and possibly to observation of more open conformations.

Acknowledgments

We are grateful to Dr. Sean Gay for critical reading of the manuscript, and we also thank the staff at Stanford Synchrotron Radiation Lightsource, operated by Stanford University on behalf of the U.S. Department of Energy, Office of Basic Energy Sciences for assistance with data collection. The Stanford Synchrotron Radiation Lightsource is supported by the National Institutes of Health, the National Center for Research Resources, the Biomedical Technology Program, and the U.S. Department of Energy of Biological and Environmental Research.

Authorship Contributions

Participated in research design: Shah and Halpert.
Conducted experiments: Shah and Pascual.
Contributed new reagents or analytic tools: Zhang.
Performed data analysis: Shah, Pascual, and Stout.
Wrote or contributed to the writing of the manuscript: Shah, Stout, and Halpert.

References

- Bumpus NN and Hollenberg PF (2010) Cross-linking of human cytochrome P450 2B6 to NADPH-cytochrome P450 reductase: identification of a potential site of interaction. *J Inorg Biochem* **104**:485–488.
- Collaborative Computational Project and Number 4 (1994) The CCP4 suite: programs for protein crystallography. *Acta Crystallogr D Biol Crystallogr* **50**:760–763.
- Davis IW, Murray LW, Richardson JS, and Richardson DC (2004) MOLPROBITY:

- structure validation and all-atom contact analysis for nucleic acids and their complexes. *Nucleic Acids Res* **32**:W615–W619.
- DeLano WL (2002) *The PyMOL Molecular Graphics System* (MacPyMOL edition), DeLano Scientific, Palo Alto, CA.
- Desta Z, Saussele T, Ward B, Blievernicht J, Li L, Klein K, Flockhart DA, and Zanger UM (2007) Impact of CYP2B6 polymorphism on hepatic efavirenz metabolism in vitro. *Pharmacogenomics* **8**:547–558.
- Domanski TL and Halpert JR (2001a) Analysis of mammalian cytochrome P450 structure and function by site-directed mutagenesis. *Curr Drug Metab* **2**:117–137.
- Domanski TL, He YA, Harlow GR, and Halpert JR (2000) Dual role of human cytochrome P450 3A4 residue Phe-304 in substrate specificity and cooperativity. *J Pharmacol Exp Ther* **293**:585–591.
- Domanski TL, He YQ, Scott EE, Wang Q, and Halpert JR (2001b) The role of cytochrome 2B1 substrate recognition site residues 115, 294, 297, 298, and 362 in the oxidation of steroids and 7-alkoxycoumarins. *Arch Biochem Biophys* **394**:21–28.
- Domanski TL, Liu J, Harlow GR, and Halpert JR (1998) Analysis of four residues within substrate recognition site 4 of human cytochrome P450 3A4: role in steroid hydroxylase activity and α -naphthoflavone stimulation. *Arch Biochem Biophys* **350**:223–232.
- Emsley P and Cowtan K (2004) Coot: model-building tools for molecular graphics. *Acta Crystallogr D Biol Crystallogr* **60**:2126–2132.
- Gay SC, Roberts AG, and Halpert JR (2010a) Structural features of cytochromes P450 and ligands that affect drug metabolism as revealed by X-ray crystallography and NMR. *Future Med Chem* **2**:1451–1468.
- Gay SC, Roberts AG, Maekawa K, Talakad JC, Hong WX, Zhang Q, Stout CD, and Halpert JR (2010b) Structures of cytochrome P450 2B4 complexed with the antiplatelet drugs ticlopidine and clopidogrel. *Biochemistry* **49**:8709–8720.
- Gay SC, Shah MB, Talakad JC, Maekawa K, Roberts AG, Wilderman PR, Sun L, Yang JY, Huelga SC, Hong WX, et al. (2010c) Crystal structure of a cytochrome P450 2B6 genetic variant in complex with the inhibitor 4-(4-chlorophenyl)imidazole at 2.0-Å resolution. *Mol Pharmacol* **77**:529–538.
- Gay SC, Zhang H, Wilderman PR, Roberts AG, Liu T, Li S, Lin HL, Zhang Q, Woods VL Jr, Stout CD, et al. (2011) Structural analysis of mammalian cytochrome P450 2B4 covalently bound to the mechanism-based inactivator *tert*-butylphenylacetylene: insight into partial enzymatic activity. *Biochemistry* **50**:4903–4911.
- Hanna IH, Reed JR, Guengerich FP, and Hollenberg PF (2000) Expression of human cytochrome P450 2B6 in *Escherichia coli*: characterization of catalytic activity and expression levels in human liver. *Arch Biochem Biophys* **376**:206–216.
- Harlow GR and Halpert JR (1997) Alanine-scanning mutagenesis of a putative substrate recognition site in human cytochrome P450 3A4. Role of residues 210 and 211 in flavonoid activation and substrate specificity. *J Biol Chem* **272**:5396–5402.
- He Y, Luo Z, Klekotka PA, Burnett VL, and Halpert JR (1994) Structural determinants of cytochrome P450 2B1 specificity: evidence for five substrate recognition sites. *Biochemistry* **33**:4419–4424.
- Holmans PL, Shet MS, Martin-Wixtrom CA, Fisher CW, and Estabrook RW (1994) The high-level expression in *Escherichia coli* of the membrane-bound form of human and rat cytochrome b₅ and studies on their mechanism of function. *Arch Biochem Biophys* **312**:554–565.
- Johnson EF and Stout CD (2005) Structural diversity of human xenobiotic-metabolizing cytochrome P450 monooxygenases. *Biochem Biophys Res Commun* **338**:331–336.
- Kleywegt GJ and Jones TA (1994) Detection, delineation, measurement and display of cavities in macromolecular structures. *Acta Crystallogr D Biol Crystallogr* **50**:178–185.
- Kobayashi Y, Strobel SM, Hopkins NE, Alworth WL, and Halpert JR (1998) Catalytic properties of an expressed cytochrome P450 2B1 from a Wistar-Kyoto rat liver cDNA library. *Drug Metab Dispos* **26**:1026–1030.
- Korhonen LE, Turpeinen M, Rahnasto M, Wittekindt C, Poso A, Pelkonen O, Raunio H, and Juvonen RO (2007) New potent and selective cytochrome P450 2B6 (CYP2B6) inhibitors based on three-dimensional quantitative structure-activity relationship (3D-QSAR) analysis. *Br J Pharmacol* **150**:932–942.
- Kumar S, Zhao Y, Sun L, Negi SS, Halpert JR, and Muralidhara BK (2007) Rational engineering of human cytochrome P450 2B6 for enhanced expression and stability: importance of a Leu264→Phe substitution. *Mol Pharmacol* **72**:1191–1199.
- Leslie AG (1999) Integration of macromolecular diffraction data. *Acta Crystallogr D Biol Crystallogr* **55**:1696–1702.
- Lindberg RL and Negishi M (1991) Modulation of specificity and activity in mammalian cytochrome P-450. *Methods Enzymol* **202**:741–752.
- Long F, Vagin AA, Young P, and Murshudov GN (2008) BALBES: a molecular-replacement pipeline. *Acta Crystallogr D Biol Crystallogr* **64**:125–132.
- Mitsuda M and Iwasaki M (2006) Improvement in the expression of CYP2B6 by co-expression with molecular chaperones GroES/EL in *Escherichia coli*. *Protein Expr Purif* **46**:401–405.
- Murshudov GN, Vagin AA, and Dodson EJ (1997) Refinement of macromolecular structures by the maximum-likelihood method. *Acta Crystallogr D Biol Crystallogr* **53**:240–255.
- Omura T and Sato R (1964) The carbon monoxide-binding pigment of liver microsomes. Evidence for its hemoprotein nature. *J Biol Chem* **239**:2370–2378.
- Scott EE, Spatzenegger M, and Halpert JR (2001) A truncation of 2B subfamily cytochromes P450 yields increased expression levels, increased solubility, and decreased aggregation while retaining function. *Arch Biochem Biophys* **395**:57–68.
- Scott EE, White MA, He YA, Johnson EF, Stout CD, and Halpert JR (2004) Structure of mammalian cytochrome P450 2B4 complexed with 4-(4-chlorophenyl)imidazole at 1.9-Å resolution: insight into the range of P450 conformations and the coordination of redox partner binding. *J Biol Chem* **279**:27294–27301.
- Segel IH (1975) *Enzyme Kinetics: Behavior and Analysis of Rapid Equilibrium and Steady-State Enzyme Systems*, Wiley-Interscience, New York.
- Soltis SM, Cohen AE, Deacon A, Eriksson T, González A, McPhillips S, Chui H, Dunten P, Hollenbeck M, Mathews I, et al. (2008) New paradigm for macromolec-

- ular crystallography experiments at SSRL: automated crystal screening and remote data collection. *Acta Crystallogr D Biol Crystallogr* **64**:1210–1221.
- van Aalten DM, Bywater R, Findlay JB, Hendlich M, Hooft RW, and Vriend G (1996) PRODRG, a program for generating molecular topologies and unique molecular descriptors from coordinates of small molecules. *J Comput Aided Mol Des* **10**:255–262.
- Wilderman PR, Shah MB, Liu T, Li S, Hsu S, Roberts AG, Goodlett DR, Zhang Q, Woods VL Jr, Stout CD, et al. (2010) Plasticity of cytochrome P450 2B4 as investigated by hydrogen-deuterium exchange mass spectrometry and x-ray crystallography. *J Biol Chem* **285**:38602–38611.
- Williams PA, Cosme J, Sridhar V, Johnson EF, and McRee DE (2000) Mammalian microsomal cytochrome P450 monooxygenase: structural adaptations for membrane binding and functional diversity. *Mol Cell* **5**:121–131.
- Zanger UM, Klein K, Saussele T, Bliedernicht J, Hofmann MH, and Schwab M (2007) Polymorphic CYP2B6: molecular mechanisms and emerging clinical significance. *Pharmacogenomics* **8**:743–759.
- Zhang H, Sridar C, Kenaan C, Amunugama H, Ballou DP, and Hollenberg PF (2011) Polymorphic variants of cytochrome P450 2B6 (CYP2B6.4–CYP2B6.9) exhibit altered rates of metabolism for bupropion and efavirenz: a charge-reversal mutation in the K139E variant (CYP2B6.8) impairs formation of a functional P450-reductase complex. *J Pharmacol Exp Ther* **338**:803–809.
- Zhang Q, Ma X, Ward A, Hong WX, Jaakola VP, Stevens RC, Finn MG, and Chang G (2007) Designing facial amphiphiles for the stabilization of integral membrane proteins. *Angew Chem Int Ed Engl* **46**:7023–7025.
- Zhao Y, Sun L, Muralidhara BK, Kumar S, White MA, Stout CD, and Halpert JR (2007) Structural and thermodynamic consequences of 1-(4-chlorophenyl)imidazole binding to cytochrome P450 2B4. *Biochemistry* **46**:11559–11567.

Address correspondence to: Dr. Manish B. Shah, Skaggs School of Pharmacy and Pharmaceutical Sciences, University of California, San Diego, 9500 Gilman Dr. #0703, La Jolla, CA 92093-0703. E-mail: m7shah@ucsd.edu
